

Adaptive Scales of Spatial Integration and Response Latencies in a Critically-Balanced Model of the Primary Visual Cortex

Keith Hayton, Dimitrios Mourogiannis, and Marcelo Magnasco
Laboratory of Integrative Neuroscience, The Rockefeller University

(Dated: May 18, 2022)

The brain processes visual inputs having structure over a large range of spatial scales. The precise mechanisms or algorithms used by the brain to achieve this feat are largely unknown and an open problem in visual neuroscience. In particular, the spatial extent in visual space over which primary visual cortex (V1) performs evidence integration has been shown to change as a function of contrast and other visual parameters, thus adapting scale in visual space in an input-dependent manner. We demonstrate that a simple dynamical mechanism—dynamical criticality—can simultaneously account for the well-documented input-dependence characteristics of three properties of V1: scales of integration in visuotopic space, extents of lateral integration on the cortical surface, and response latencies.

The characteristics of stimuli in the natural world vary over staggering ranges. Our nervous system evolved within this environment to parse such widely-ranging stimuli, and research into how the nervous system can cope with such ranges has led to considerable advances in our understanding of neural circuitry. For example at the sensory transduction level, the physical magnitudes encoded into primary sensors, such as light intensity, sound pressure level and olfactant concentration, vary over exponentially-large ranges; as neuronal firing rates cannot similarly vary over decades, the encoding process must compress such ranges, leading to the Weber-Fechner laws. This stimulated a large amount of research into the mechanisms through which physical stimuli are *non-linearly compressed* into the far more limited ranges of neural activity that represent them [1]. Of relevance to our later discussion is the nonlinear compression of sound intensity in the early auditory pathways [2, 3], where it has been shown that poisoning the active cochlear elements on a Hopf bifurcation leads to cubic-root compression.

But other characteristics besides the raw physical magnitude still vary hugely. The wide range of spatial extents and correlated linear structures present in visual scenery [4–6] present a more subtle problem, if we think of the visual areas as fundamentally limited by their underlying physical connectivity. Studies of primary visual cortex (V1) have found that as the contrast of a stimulus is decreased, the extent over which the input is integrated increases (Fig 1) [7, 8]. More specifically, while the classical receptive field is the area in visual space over which a small linear segment elicits a response, the *extraclassical receptive field* of V1 neurons is defined as the area in visual space within which *additional* input changes the neuronal response, e.g. the area over which increasing the extent of a line changes firing rates [7–10]; these findings thus demonstrated that the extraclassical receptive fields in V1 are not constant but instead grow and shrink according to stimulus contrast. Thus the "computation" being carried out is not fixed but is itself a function of the input.

Let us examine this distinction carefully. There are numerous operations in image processing, such as Gaussian blurs or other *convolutional kernels*, whose spatial range is fixed. It is very natural to imagine neural circuitry having actual physical connections corresponding to the nonzero elements of a convolutional kernel, and in fact a fair amount of effort has been expended trying to identify actual synapses corresponding to such elements [11, 12]. There are, however, other image-processing operations, such as floodfill (the "paint bucket") whose spatial extent is entirely dependent on the input; the problem of "binding" of perceptual elements is usually thought about in this way, and mechanisms posited to underlie such propagation dynamics include synchronization of oscillations acting in a vaguely paint-bucket-like way [13–15]. This dichotomy is artificial because these are only the two extremes of a potentially continuous range. While the responses of neurons in V1 superficially appear to be convolutional kernels, their strong dependence on input characteristics, particularly the size of the extra-classical receptive field, demonstrates a more complex logic in which spatial extent is determined by specific characteristics of the input. What is the circuitry underlying this logic?

Neurons in the primary visual cortex are laterally connected to other neurons on the cortical surface and derive input from them. Experiments have shown that the spatial extent *on the cortical surface* from which neurons derive input from other neurons through such lateral interactions varies with the contrast of the stimulus [16]. In the absence of stimulus contrast, spike-triggered traveling waves of activity propagate over large areas of cortex. As contrast is increased, the waves become weaker in amplitude and travel over increasingly small distances. These experiments suggested that the change in spatial summation area with increasing stimulus contrast may be consistent with the change in the decay constants of the traveling wave activity. However no extant experiment directly links changes in summation in visual space to changes in integration on the cortical surface, and no explicit model of neural architecture has been shown to

simultaneously account for, and thus connect, the input-dependence of spatial summation and lateral integration in V1. The latter one is our aim, and a crucial clue will come from the input-dependence of latencies.

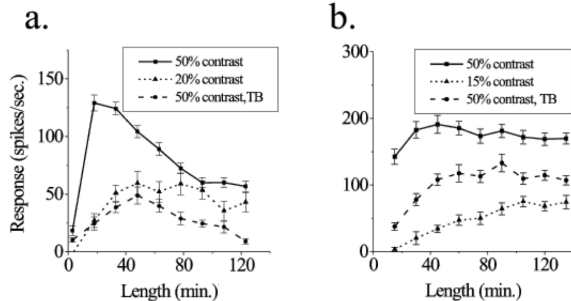


Figure 1. **Reprinted from [7] with permission: Copyright (1999) National Academy of Sciences, U.S.A. Measurements of single-neuron responses in the V1 area of monkeys to optimally oriented bars of light of different lengths and contrasts.** Panels a and b are measurements from two distinct neurons. The units of length along the horizontal axis are in minutes of arc. The solid, dotted, and dashed curves represent bars of light of 50% contrast, 15% contrast, and 50% contrast embedded in a textured background, respectively. The dashed curves are irrelevant to the focus of this paper.

Recently, a dynamically critically-poised network model of cortex was proposed to explain the contrast dependence of functional connectivity [17]. It was shown that in the absence of input, the model exhibits wave-like activity with an infinitely-long ranged susceptibility, while in the presence of input, perturbed network activity decays exponentially with an attenuation constant that increases with the strength of the input. These results are in direct agreement with Nauhaus *et al* [16].

We will now demonstrate that similar critically-balanced network models also lead to adaptive scales of spatial integration in visual space. Our model makes two key assumptions. The first is a local, not just global, balance of excitation and inhibition across the entire network; all eigenmodes of the network are associated with purely imaginary eigenvalues. It has been shown that such a critically-balanced configuration can be achieved by evolving a network of neurons with connections evolving under an anti-Hebbian rule [18]. The second key assumption is that all interactions in the network are local and described by the connectivity matrix; nonlinearities do not couple distinct neurons in the network.

There are a number of examples of dynamical criticality in neuroscience, including theoretical [19] and experimental studies [20] of line attractors in oculomotor control, line attractors in decision making [21], Hopf bifurcation in the auditory periphery [22] and olfactory system [23], and theoretical work on regulated criticality [24]. More recently, Solovey *et al.* [25] performed stability analysis of high-density electrocorticography recordings

covering an entire cerebral hemisphere in monkeys during reversible loss of consciousness. Performing a moving vector autoregressive analysis of the activity, they observe that the eigenvalues crowd near the critical line. During loss of consciousness, the numbers of eigenmodes at the edge of instability decrease smoothly but drift back to the critical line during recovery of consciousness.

We will also examine the dynamics of the critically-balanced model and show that the system exponentially decays to its steady state over multiple timescales that flexibly adapt to the strength of the input. Specifically, we find that the temporal exponential decay constants increase with increasing input strength. This result agrees with single-neuron studies which have found that response latencies in V1 decrease with increasing stimulus contrast [7, 26–28]. We now turn to describing our model.

Let $x \in \mathbb{C}^N$ be the activity vector for a network of neurons which evolve in time according to the normal form equation

$$\dot{x}_i = \sum_j A_{ij} x_j - |x_i|^2 x_i + I_i(t) \quad (1)$$

In this model, originally proposed by Yan and Magnasco [17], neurons interact with one another through a skew-symmetric connectivity matrix A . The cubic/nonlinear term in the model is purely local and does not couple the activity states of distinct neurons, while the external input, $I(t) \in \mathbb{C}^N$, to the system may depend on time and have a complex spatial pattern.

The original model considered a 2-D checkerboard topology of excitatory and inhibitory neurons. For theoretical simplicity and computational ease, we will instead consider a 1-D checkerboard layout of excitatory and inhibitory neurons which interact through equal strength, nearest neighbor connections (Figure (2)). In this case, $A_{ij} = (-1)^j s(\delta_{i,j+1} + \delta_{i,j-1})$, where $i, j = 0, 1, \dots, N-1$ and s is the synaptic strength. Boundary conditions are such that the activity terminates to 0 outside of the finite network.



Figure 2. **Simplest connectivity matrix A .** A finite line of excitatory and inhibitory neurons. White nodes represent excitatory neurons. Black nodes are inhibitory. The connection strength of each neuron is identical.

We are specifically interested in the time-asymptotic response of the system, but explicitly integrating the stiff, high-dimensional ODE in (1) is difficult. Fortunately, we can bypass numerical integration methods by assuming periodic input of the form $I(t) = F e^{i\omega t}$ where $F \in \mathbb{C}^N$

and look for solutions $X(t) = Ze^{i\omega t}$ where $Z \in \mathbb{C}^N$. Substituting these into (1), we find that

$$g(Z) := (A - i\omega)Z - |Z|^2 Z + F = 0 \quad (2)$$

The solution of (2) can be found numerically by using the multivariable Newton-Raphson method in the complex plane:

$$\tilde{Z} \rightarrow \tilde{Z} - J(\tilde{Z})^{-1} \tilde{g}(Z) \quad (3)$$

where $\tilde{Z} := (z_1, z_2) = (\text{Re}(Z), \text{Im}(Z))$, $\tilde{g}(Z) := (g_1(Z), g_2(Z)) = (\text{Re}(g(Z)), \text{Im}(g(Z)))$, and J is the Jacobian of \tilde{g} with respect to \tilde{Z} :

$$J_{ij}(z) = \frac{\partial g_i}{\partial z_j}$$

To test how the response of a single neuron in the network varies with both the strength and length of the input, we select a center neuron at index c and then calculate, for a range of input strengths, the response of the neuron as a function of input length around it. Formally, for each input strength level $B \in \mathbb{R}$, we solve (3) for

$$F_k(B, l) = \begin{cases} Bv_k & \text{if } k \in [c-l, c+l] \\ 0 & \text{otherwise} \end{cases} \quad (4)$$

where $k = 1, \dots, N$, $v \in \mathbb{C}^N$ describes the the spatial shape of the input, and $2l + 1$ is the length of the input in number of neurons. The response of the center neuron is taken as the modulus of Z_c , where Z is the activity vector, and we focus on the case where ω is an eigenfrequency of A and v the corresponding eigenvector.

The result for a 1-D checkerboard network of 64 neurons is shown in Figure 3. Here we fix a center neuron and sweep across a small range of eigenfrequencies ω of A . The curves from bottom to top correspond to an ascending order of base-2 exponentially distributed input strengths $C = 2^i$. For all eigenfrequencies, the peak of the response curves shift towards larger input lengths as the input strength decreases. In fact, for very weak input, the response curves rise monotonically over the entire range of input lengths without ever reaching a maximum in this small finite network. This is in contrast to the strong input response curves, which always reach a maximum but, depending on the eigenfrequency, exhibit varying degrees of response suppression beyond it. This is consistent with variability of response suppression in primary visual cortex studies [7, 8]. In Figure 3, eigenfrequencies $\omega = 1.92, 1.96, 1.99$ show the greatest amount of suppression while the others display little to none.

To understand why certain eigenfrequencies lead to suppression, we fix the eigenfrequency to be $\omega = 1.92$ and examine the response curves of different center neurons. The response of four center neurons (labeled by network position) and the modulus of the eigenfrequency's

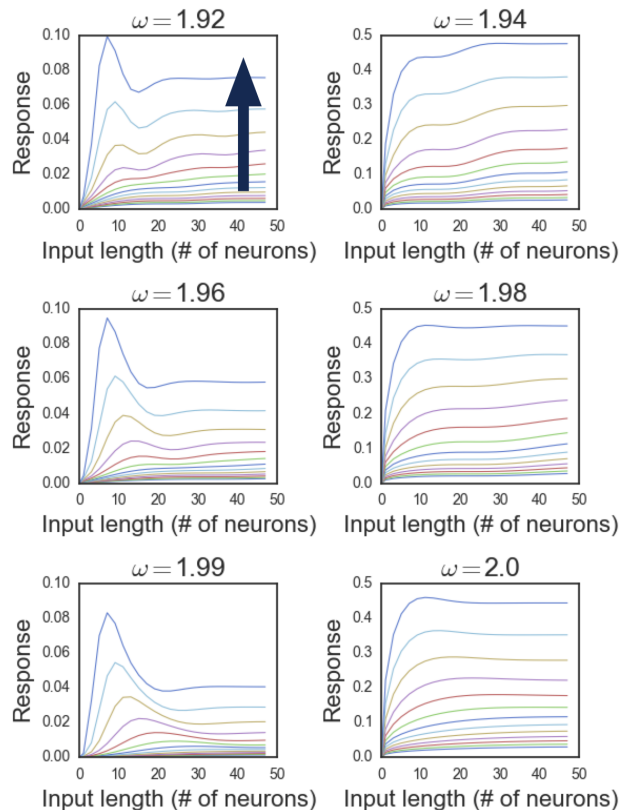


Figure 3. **Length-response curves for different eigenfrequencies.** In each panel, which corresponds to a different eigenfrequency of A , we plot the response of the neuron as a function of input length for a group of exponentially distributed input strengths. The blue arrow in the first plot indicates the direction of increasing input strength. The length of the input is recorded in number of neurons and the response is taken as the modulus of the amplitude of the time-asymptotic stable limit cycle.

corresponding eigenvector are plotted in Figure 4. The center neurons closest to the zeros of the eigenvector experience the strongest suppression for long line lengths. Neuron 38 closer to the peak of the eigenvector's modulus experiences almost zero suppression. This generally holds for all eigenvectors and neurons in the network as all eigenvectors are periodic in their components with an eigenvalue-dependent spatial frequency.

To strengthen the connection between model and neurophysiology, one can consider a critically-balanced network with an odd number of neurons so that 0 is now an eigenfrequency of the system. In our model, input associated with the 0-eigenmode represents direct current input to the system which is what neurophysiologists utilize in experiments; the visual input is not flashed. To achieve surround suppression in the network, one only needs to add appropriately chosen long range connections to the nearest neighbor connectivity.

Next, we show that the network not only selectively integrates input as a function of input strength but also

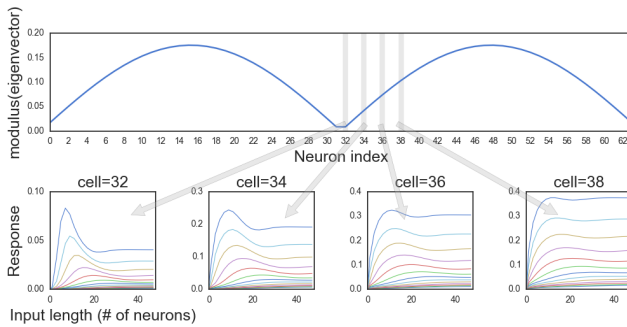


Figure 4. **Length-response curves of different neurons.** The top plot depicts the modulus of the eigenvector corresponding to eigenfrequency $\omega = 1.92$. The 4 panels below are plots of the length-response curves for 4 different neurons in the network. The position of the neurons relative to the shape of the eigenvector are noted with the gray bars and arrows.

operates on multiple time scales which flexibly adapt to the input. This behavior is not surprising given that in the case of a single critical Hopf oscillator, the half width of the resonance, the frequency range for which the oscillator’s response falls by a half, is proportional to the forcing strength of the input, $\Gamma \propto F^{\frac{2}{3}}$ where Γ is the half-width F the input strength [3]. Thus, decay constants in the case of a single critical oscillator should grow with the input forcing strength as $F^{\frac{2}{3}}$.

Assuming input with eigenfrequency ω and corresponding eigenvector v , as described above, the network activity $X(t)$ decays exponentially in time to a stable limit cycle, $X(t) = Ze^{i\omega t}$. This implies that for any neuron i in the network, $|X_i(t)| = e^{-bt}f(t) + |Z_i|$ during the approach to the limit cycle. We therefore plot $\log(|X_i(t)| - |Z_i|)$ over the transient decay period and estimate the slope of the linear regimes. We do this for

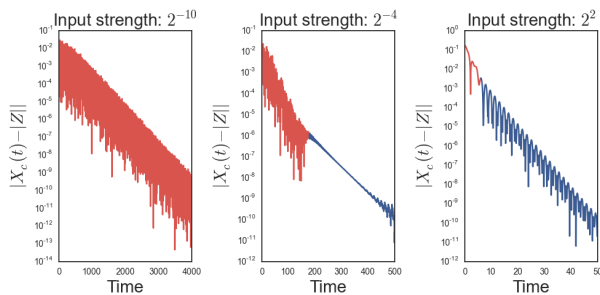


Figure 5. **Input-strength-dependent timescales.** For neuron i in the network, we plot $\log(|X_i(t)| - |Z_i|)$ as a function of time for 3 different input strengths. Linear regions correspond to exponential decay. In the presence of weak input, a fast decay regime (red) guides the dynamics towards a stable limit cycle. For the intermediate input strength, a new, distinct slow decay regime appears (blue), which becomes dominant for strong input

a nearly network size input length ($L = 29$, $N = 32$)

and a range of exponentially distributed input strengths. In Figure 5, we plot representative transient periods of a single neuron corresponding to 3 input strengths: 2^{-10} , 2^{-4} , and 2^2 . For weak input there is a fast single exponential decay regime (red) that determines the system’s approach to the stable limit cycle. As we increase the input, however, the transient period displays two exponential decay regimes: the fast decay regime (red) which was observed in the presence of weak input and a new slow decay regime (blue) immediately preceding the stable limit cycle. For very large input strength, the slow decay regime becomes dominant. The multiple decay regimes is a surprising result which doesn’t appear in the case of a single critical Hopf oscillator.

We estimate the exponential decay constants as a function of input strength and plot them on a log-log scale in Figure 6. The red circles correspond to the fast decay regime, while the blue circles correspond to the slow decay regime, which becomes prominent for larger forcings. We separately fit both the slow and fast decay regimes with a best fit line. Unsurprisingly, the slopes of the lines are equal and approximately $\frac{2}{3}$. Thus, the decay constants grow with the input as $\propto F^{\frac{2}{3}}$, where F is the input strength. Thus the system operates on multiple timescales dynamically switching from one to another depending on the magnitude of the forcing. The larger the forcing, the faster the network response.

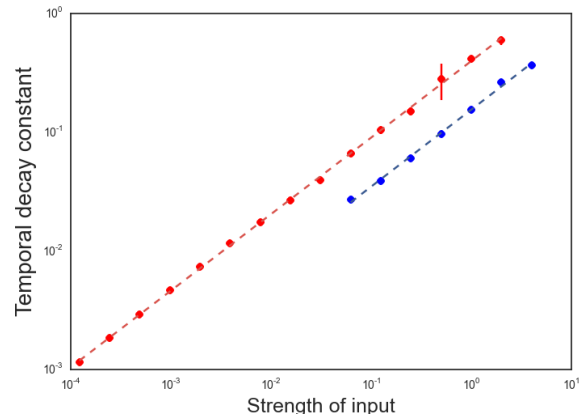


Figure 6. **Input-strength dependence of exponential decay constants.** The temporal exponential decay constants for a range of input strengths is depicted above. A fast decay regime (red circles) is accompanied by a slow decay regime (blue circles) at large input strengths. Each decay regime is separately approximated by a least squares line (dashed lines) in log-log space.

In this paper, we consider a line of excitatory and inhibitory neurons, but our results hold equally well for a ring of neurons with periodic boundary conditions and appropriately chosen long range connections. Ring networks have previously been used to model orientation selectivity in V1. In agreement with recent findings, the

critically-balanced ring network exhibits surround suppression in orientation space when long range connections are added on top of the nearest neighbor connectivity.

We have shown that a simple dynamical system poised at the onset of instability exhibits an input-strength dependent scale of integration of the system's input and input-strength dependent response latencies. This finding strongly complements our previous results showing that a similar nonlinear process with fixed, nearest neighbor network connectivity leads to input-dependent functional connectivity. This system is thus the first proposed mechanism that can account for contrast dependence of spatial summation, functional connectivity, and response latencies. In this framework, these three characteristic properties of signal processing in V1 are intrinsically linked to one another.

-
- [1] E. R. Kandel, J. H. Schwartz, T. M. Jessell, S. A. Siegelbaum, and A. J. Hudspeth, *Principles of neural science, 4th Edition* (McGraw-hill New York, 2000).
- [2] S. Camalet, T. Duke, F. Jülicher, and J. Prost, Proc. Natl. Acad. Sci. U.S.A. **97**, 3183 (2000).
- [3] V. M. Eguíluz, M. Ospeck, Y. Choe, A. Hudspeth, and M. O. Magnasco, Phys. Rev. Lett. **84**, 5232 (2000).
- [4] M. Sigman, G. A. Cecchi, C. D. Gilbert, and M. O. Magnasco, Proc. Natl. Acad. Sci. U.S.A. **98**, 1935 (2001).
- [5] D. J. Field, JOSA A **4**, 2379 (1987).
- [6] D. L. Ruderman and W. Bialek, Phys. Rev. Lett. **73**, 814 (1994).
- [7] M. K. Kapadia, G. Westheimer, and C. D. Gilbert, Proc. Natl. Acad. Sci. U.S.A. **96**, 12073 (1999).
- [8] M. P. Sceniak, D. L. Ringach, M. J. Hawken, and R. Shapley, Nature Neuroscience **2**, 733 (1999).
- [9] G. C. DeAngelis, R. D. Freeman, and I. Ohzawa, J. Neurophysiology **71**, 347 (1994).
- [10] G. DeAngelis, J. Robson, I. Ohzawa, and R. Freeman, J. Neurophysiology **68**, 144 (1992).
- [11] B. A. Olshausen and D. J. Field, Nature **381**, 607 (1996).
- [12] R. C. Reid and J.-M. Alonso, Nature **378**, 281 (1995).
- [13] F. Rosenblatt, *Principles of neurodynamics. perceptrons and the theory of brain mechanisms*, Tech. Rep. (DTIC Document, 1961).
- [14] C. Von der Malsburg, Neuron **24**, 95 (1999).
- [15] T. S. Lee and D. Mumford, JOSA A **20**, 1434 (2003).
- [16] I. Nauhaus, L. Busse, M. Carandini, and D. L. Ringach, Nature Neuroscience **12**, 70 (2009).
- [17] X.-H. Yan and M. O. Magnasco, PloS one **7**, e41419 (2012).
- [18] M. O. Magnasco, O. Piro, and G. A. Cecchi, Phys. Rev. Lett. **102**, 258102 (2009).
- [19] H. S. Seung, Neural Networks **11**, 1253 (1998).
- [20] H. S. Seung, D. D. Lee, B. Y. Reis, and D. W. Tank, Neuron **26**, 259 (2000).
- [21] C. K. Machens, R. Romo, and C. D. Brody, Science **307**, 1121 (2005).
- [22] Y. Choe, M. O. Magnasco, and A. Hudspeth, Proc. Natl. Acad. Sci. U.S.A. **95**, 15321 (1998).
- [23] W. J. Freeman and M. D. Holmes, Neural Networks **18**, 497 (2005).
- [24] E. Bienenstock and D. Lehmann, Adv in Complex Syst **1**, 361 (1998).
- [25] G. Solovey, L. M. Alonso, T. Yanagawa, N. Fujii, M. O. Magnasco, G. A. Cecchi, and A. Proekt, J. Neuroscience **35**, 10866 (2015).
- [26] M. Carandini, D. J. Heeger, *et al.*, Science-AAAS-Weekly Paper Edition-including Guide to Scientific Information **264**, 1333 (1994).
- [27] T. J. Gawne, T. W. Kjaer, and B. J. Richmond, J. Neurophysiology **76**, 1356 (1996).
- [28] D. G. Albrecht, W. S. Geisler, R. A. Frazor, and A. M. Crane, J. Neurophysiology **88**, 888 (2002).